Collapse of the charge disproportionation and covalency-driven insulator-metal transition in $Sr_3Fe_2O_7$ under pressure

P. Adler, U. Schwarz,* and K. Syassen

Max-Planck-Institut für Festkörperforschung, Heisenbergstrasse 1, D-70569 Stuttgart, Germany

G. Kh. Rozenberg, G. Yu. Machavariani, A. P. Milner, and M. P. Pasternak

School of Physics and Astronomy, Tel Aviv University, 69978 Tel Aviv, Israel

M. Hanfland

European Synchrotron Radiation Facility, Boîte Postale 220, F-38043 Grenoble, France

The effect of pressure on electronic properties and crystal structure of $Sr_3Fe_2O_7$ was studied up to 45 GPa. Experimental methods employed were ^{57}Fe Mössbauer spectroscopy (MS), monochromatic synchrotron powder x-ray diffraction, optical reflectance between 0.6 and 4 eV, and electrical resistance measurements. Mössbauer spectra of the magnetically ordered as well as of the paramagnetic phase demonstrate that the charge disproportionation of Fe^{IV} disappears at pressures between 15 and 21 GPa. The diffraction data show that the tetragonal Ruddlesden-Popper-type crystal structure (space group $I4/mmm$) is retained up to the highest pressure. The optical spectra reveal a continuous increase with pressure of the near-infrared oscillator strength, which indicates a pressure-driven transition from an insulating towards a metallic ground state. This is confirmed by the electrical resistance measurements which evidence a sluggish pressure-induced insulator-metal (IM) transition with a clear incipient metallic state at $P \approx 20$ GPa. The changes in electronic state are not associated with any detectable anomaly in the pressure dependence of lattice parameters. The high-pressure behavior of $Sr_3Fe_2O_7$ is discussed in terms of a strengthening of the covalent $Fe(3d)$-$O(2p)$-$Fe(3d)$ interactions under pressure. Within the impurity model for the electronic structure of transition metal compounds the IM transition in $Sr_3Fe_2O_7$ can be attributed to the closure of a p-p-type energy gap. The ambient- and high-pressure properties of $Sr_3Fe_2O_7$ and related Fe^{IV} oxides are compared. [S0163-1829(99)10531-9]

I. INTRODUCTION

The interplay between chemical composition, crystal structure, electronic structure, magnetism, and electrical transport behavior of transition metal (TM) compounds has been studied extensively in recent years.[1] One class of materials of current interest are the mixed-valence Mn^{III}/Mn^{IV} oxomanganates, e.g., $Ln_{1-x}M_xMnO_3$ with $M=Ca,Sr$, where a negative colossal magnetoresistance effect near the transition from a ferromagnetic metallic state to a paramagnetic semiconducting state is observed.[2–5] The parent compound $LaMnO_3$ is an insulator with a distorted perovskite structure and A-type antiferromagnetic ordering.[6,7] The orthorhombic crystal structure of $LaMnO_3$ reflects a cooperative Jahn-Teller effect arising from the $t_{2g}^3 e_g^1$ electronic configuration of Mn^{III} in an octahedral environment of oxygen ions.

A wide variety of electronic properties is encountered in oxides with isoelectronic Fe^{IV} ions.[8] For instance, in contrast to $LaMnO_3$ the Fe^{IV} oxide $SrFeO_3$ remains a cubic perovskite even at low temperatures with regular FeO_6 octahedra, a metalliclike conductivity, and magnetic ordering with a helical spin structure.[9–11] Trends in the electronic properties of perovskite-related TM oxides often can be rationalized by considering the strength of covalent $TM(3d)$-$O(2p)$-$TM(3d)$ interactions in relation to the effective on-site correlation (Coulomb and exchange) energy U.[12] It is reasonable to assume that the t_{2g} electrons are

localized as they are only involved in rather weak $\pi^*[t_2 - O(2p_\pi)-t_2]$ interactions. The stronger $\sigma^*[e - O(2s,2p_\sigma)-e]$ interactions lead to the formation of a σ^* conduction band of width w_σ which for TM ions having formally a d^4 high-spin configuration is quarter filled in the metallic limit. The different electronic and structural properties of $LaMnO_3$ and $SrFeO_3$, in particular the suppression of the Jahn-Teller effect in $SrFeO_3$, arise from the larger itinerancy of the σ^* electrons in the Fe^{IV} oxides which is a consequence of the stronger covalency of Fe-O bonding. The analysis of the electronic structure of $SrFeO_3$ within a cluster model suggests that the insulating as well as the metallic ground states of Fe^{IV} oxides are dominated by d^5L^{-1} rather than by ionic d^4 configurations.[13] L^{-1} refers to a hole in the oxygen p bands. Accordingly, it is believed that the lowest-energy excitation gap in these compounds is neither of the Mott-Hubbard nor of the charge transfer but of p-p type.

$SrFeO_3$ is the $n=\infty$ member of a Ruddlesden-Popper-type series of compounds with the general formula $Sr_{n+1}Fe_nO_{3n+1}$. The $n=1$ member Sr_2FeO_4 has the K_2NiF_4-type crystal structure. It is an antiferromagnetic semiconductor with several nonequivalent Fe^{4+} sites seen in the Mössbauer spectra of the magnetically ordered phase.[14,15] The spectra have been interpreted in terms of a spiral spin arrangement.[15] An oxygen-derived phonon band in the Raman spectra of Sr_2FeO_4 occurring near 380 cm^{-1} at 20 K which is not intrinsic to the K_2NiF_4-type crystal structure
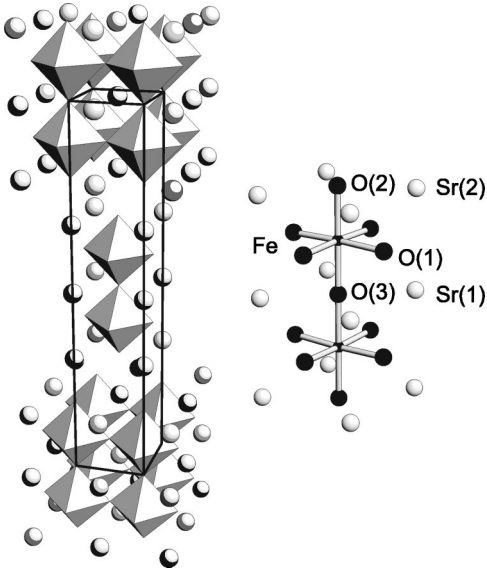
FIG. 1. View of the crystal structure of $Sr_3Fe_2O_7$ and the labeling scheme for the atoms.

suggests the possibility of a small structural distortion.[16]

The crystal structure of the $n=2$ member $Sr_3Fe_2O_7$ reveals double layers of corner-sharing FeO_6 units stacked along the c axis of the tetragonal lattice (space group $I4/mmm$), as schematically indicated in Fig. 1. Mössbauer spectra[15,17] of this semiconducting compound, which orders antiferromagnetically below $T_N \approx 110$ K, evidence a charge disproportionation of Fe^{IV} which may be written as

$$2Fe^{4+} \rightarrow Fe^{(4-\delta)+} + Fe^{(4+\delta)+}. \tag{1}$$
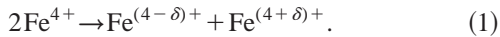
As the formal Fe oxidation state remains +4 for all members in the Ruddlesden-Popper series of strontium ferrates and as the Fe-O bond distances are quite similar, the bandwidth w_σ is mainly controlled by the degree of condensation of the Fe-O network. Accordingly, w_σ is expected to increase from Sr_2FeO_4 to $Sr_3Fe_2O_7$ to $SrFeO_3$. Another possibility for enhancing w_σ in these materials is to subject them to external pressures. High-pressure studies on Sr_2FeO_4 revealed the disappearance of the additional Raman phonon and an increase in the near-infrared optical reflectance above 5 GPa which indicates the possibility of a pressure-induced insulator-metal (IM) transition.[16] Indeed, recent resistance measurements on Sr_2FeO_4 (Ref. 18) reveal a change of the conductivity mechanism at $P \approx 6$ GPa with a final alteration from a positive to a negative temperature coefficient of the electrical conductivity near 18 GPa. In addition, the complex magnetic hyperfine pattern in the Mössbauer spectra of the magnetically ordered phase of Sr_2FeO_4 at ambient pressure collapses into a single sextet for pressures larger than about 9 GPa.[18] Preliminary high-pressure Mössbauer and energy-dispersive x-ray studies of $Sr_3Fe_2O_7$ indicate that the charge disproportionation of Fe^{IV} disappears between 10 and 20 GPa without change of the crystal structure.[19]

Here, we report a detailed investigation of the pressure dependence of electronic properties and crystal structure of $Sr_3Fe_2O_7$ up to 45 GPa employing a combination of several experimental methods. The aim of this study was to follow the pressure-induced alterations of the charge disproportion-

ation state, to investigate the possibility of a pressure-induced insulator-metal and/or high-spin to low-spin transition, and finally to correlate pressure-induced changes in electronic properties with structural properties. Indications for a high-spin to low-spin transition near 30 GPa have been reported for $CaFeO_3$,[20] which is the classical system revealing a charge disproportionation of Fe^{IV}.[21] The pressure dependence of the electronic properties of $Sr_3Fe_2O_7$ was probed by ^{57}Fe Mössbauer spectroscopy, optical reflectivity, and electrical resistance studies. In order to obtain data of sufficient quality for structure refinement the pressure dependence of the crystal structure of $Sr_3Fe_2O_7$ was studied by high-resolution angle-dispersive x-ray powder diffractometry using monochromatic synchrotron radiation.

II. EXPERIMENTAL DETAILS

Samples of $Sr_3Fe_2O_7$ were prepared from a mixture of SrO (stored under argon) and Fe_2O_3, which was ground in a ball mill, heated at $1000 °C$ overnight, pelletized, and heated for another two days at $1000 °C$. Finally, the pellets were annealed in an autoclave at an oxygen pressure of 60 MPa at $500 °C$ for 18 h and subsequently furnace cooled. For the Mössbauer studies a sample of $Sr_3Fe_2O_7$ with a ^{57}Fe content of 25% was prepared by employing a mixture of natural Fe_2O_3 and $^{57}F_2O_3$. The purity of the samples was checked by x-ray powder diffractometry. From the x-ray powder patterns the following lattice constants were derived: $a = 385.00(2)$ pm, $c = 2014.7(2)$ pm for the sample which was used for the synchrotron, optical, and resistance studies; $a = 385.38(4)$ pm, $c = 2015.1(2)$ pm for the Mössbauer sample. A neutron diffraction study on the system $Sr_3Fe_2O_{7-y}$ revealed that a is a linearly decreasing function with increasing oxygen content.[22] Since the a parameters of our samples are close to that of $Sr_3Fe_2O_{7.00(5)}$ in Ref. 15 it is concluded that the samples used in this study are not oxygen deficient.

Pressure- and temperature-dependent ^{57}Fe Mössbauer experiments were performed using a top-loading cryostat and a 10 mCi $^{57}Co(Rh)$ point source of 0.5 mm×0.5 mm area dimensions in conjunction with a $Kr-CO_2$ proportional counter; for further details see Ref. 23. All spectra were analyzed using appropriate least-squares-fitting procedures to obtain the hyperfine interaction parameters. A diamond anvil cell (DAC) with argon as pressure-transmitting medium was used for Mössbauer spectroscopy (MS) pressure studies.

Angle-dispersive powder x-ray diffraction (XRD) experiments were performed at the ID9 undulator beamline of the European Synchrotron Radiation Facility (ESRF), Grenoble. Samples of $Sr_3Fe_2O_7$ were loaded into the gasket hole of a DAC using nitrogen as the pressure-transmitting medium. Two-dimensional diffraction patterns were measured with x-ray wavelengths of 45.80 and 44.62 pm using image plate detection. In order to improve powder averaging, the DAC was rocked by $\pm 3°$. Typical exposure times were 2 to 4 min. The scanned two-dimensional images were corrected for tilt and scanner distortions and converted to intensity-vs-2Θ data using the Fit2D software.[24] Crystal structure refinements were performed using the FullProf program.[25]

Optical reflectivity spectra of $Sr_3Fe_2O_7$ between 0.6 and 4.0 eV at pressures up to 37 GPa were measured in a DAC

using a micro-optical system described in Ref. 26. Reflectivity measurements were performed under quasihydrostatic conditions, where the polycrystalline sample is in direct optical contact with a diamond window and otherwise surrounded by a transparent solid of low shear strength (CsCl in the present case). In these experiments the absolute reflectance R_d is determined for the sample-diamond interface using suitable normalization procedures.[26] With increasing pressure a smooth sample surface suitable for reflectance measurements was formed only at pressures above about 4 GPa, as is the case with many other TM oxides of high shear strength.

For resistance measurements the sample/metal-gasket cavity was coated with an insulating mixture of Al_2O_3/NaCl and epoxy. Four-probe dc resistance measurements were carried out with $5-7$-μm-thick Pt foil electrodes as a function of temperature and pressure.[27] No pressure-transmitting medium was used; the pressure distribution for the resistance studies was typically $5-10$% of the average pressure. Pressures in the MS, structural, optical, and resistance work were measured with the ruby luminescence method.[28]

III. EXPERIMENTAL RESULTS

A. Mössbauer spectroscopy

Mössbauer spectra of $Sr_3Fe_2O_7$ measured at ambient and low pressures and at $T < T_N$ reveal two equally abundant magnetic components differing in isomer shift (IS) values by 0.34 mm/s and with hyperfine field (B_{hf}) values of 26 and 39 T. This is indicative of distinct magnetic-electronic sites $Fe^{(4+\delta)+}$ and $Fe^{(4-\delta)+}$ resulting from the charge disproportionation of Fe^{IV} according to Eq. (1). These observations are in agreement with previous Mössbauer spectra of $Sr_3Fe_2O_7$ at ambient pressure.[15,17,29]

A series of high-pressure Mössbauer spectra is shown in Fig. 2. The two distinct charge states persist up to pressures of ≈ 12 GPa with B_{hf} very similar to the values at ambient pressure. Above 12 GPa the two sextets start to converge. At 15 and 18 GPa two magnetic components are still discernible, but the differences ΔB between the hyperfine fields and ΔIS between the isomer shifts have decreased considerably compared to the ambient-pressure spectra. This is supposed to signal a change in electronic structure in this pressure range. Finally, spectra at $P \geq 21$ GPa reveal a single magnetic component, indicating the stabilization of a state with a uniform charge and spin distribution, which is characterized by $B_{hf} = 27$ T and IS $= 0.02$ mm/s. The Mössbauer spectra of $Sr_3Fe_2O_7$ suggest that the δ value in Eq. (1) diminishes above 12 GPa and finally the charge disproportionation completely disappears at 21 GPa. A collapse of the charge disproportionation between 12 and 21 GPa is in agreement with the pressure dependence of the room-temperature Mössbauer spectra (not shown here) where the material is paramagnetic.

B. X-ray diffraction

Diffraction patterns of $Sr_3Fe_2O_7$ at different pressures are shown in Fig. 3. The curves shown below each diagram represent the difference between experimental and calculated data. The latter correspond to the best fits obtained from full-profile Rietveld refinement of the experimental pattern.
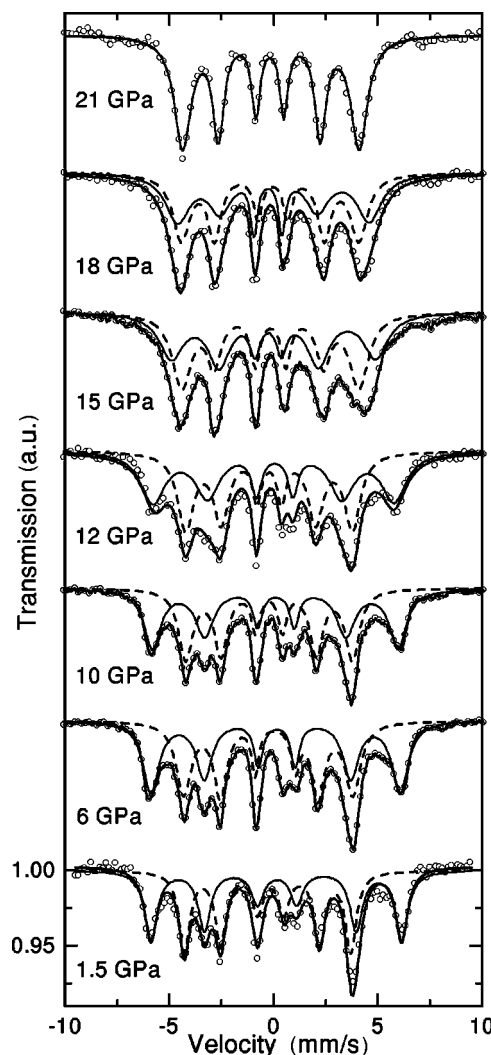
FIG. 2. ^{57}Fe Mössbauer spectra of $Sr_3Fe_2O_7$ at 50 K. The solid lines through the data points are theoretical fits. Up to ~ 18 GPa two sextets are observed which are drawn as subspectra (solid and dashed curves) and correspond to two sites. At $P \geq 21$ GPa spectra could be fitted with only one sextet. Intensities are given in normalized units.

Up to the highest pressure of 45 GPa there are no indications of a structural phase transition. All diagrams could be refined in the ambient-pressure space group $I4/mmm$. Additional weak reflections in several diagrams could be attributed to diffraction from the nitrogen matrix. A pronounced change in the relative intensities of Bragg reflections with increasing pressure is noted. This is most apparent from the intense (105) and (110) reflections whose relative intensities revert. For explaining this effect it is instructive to compare the x-ray diagrams at ambient pressure before pressurizing and after pressure release (see Fig. 3). Both diagrams agree with respect to the 2Θ values of the reflections but the changes in relative intensities are not reversible. Thus, the changes in relative intensities with increasing pressure are attributed to a continuous development of preferred orientation of the crystallites which remains after pressure release. An overall broadening of the diagram after pressure release is assigned to irreversible pressure-induced microstrain effects.

For refining the crystal structure parameters a modified Lorentzian profile function (mod 2 Lorentzian[30]) was ap-
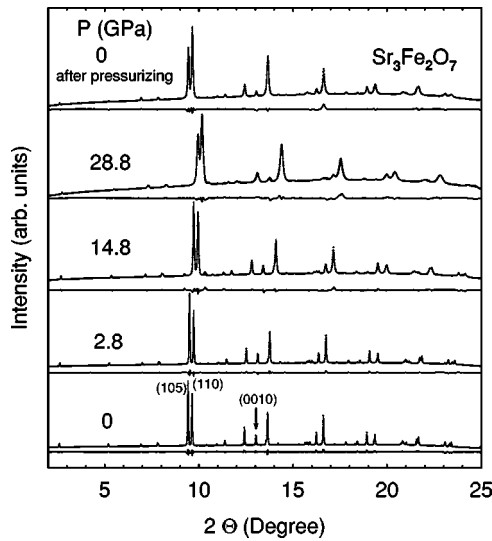
FIG. 3. Powder x-ray diffraction diagrams of $Sr_3Fe_2O_7$ at different pressures. At the bottom of each diagram the difference between experimental data and calculated profile is shown. The x-ray wavelength is 45.80 pm.

plied. The refinements included the scale factor, background, and line shape parameters, the lattice parameters a and c, four positional parameters [z-Sr(2), z-Fe, z-O(1), and z-O(2), see Fig. 1 for the labeling scheme of the atoms], and a parameter G_1 accounting for preferred orientation along the [001] axis. The preferred orientation was described by the function $P_{hkl} = \exp(-G_1 \alpha_{hkl}^2)$ where α_{hkl} is the angle between the diffraction vector and the axis of preferred orientation. Isotropic temperature factors were kept constant.

Whereas diagrams at low pressures are well reproduced, there is a misfit in the positions of the $(0,0,l)$ reflections above 10 GPa which is particularly evident for the nonoverlapping $(0,0,10)$ reflection. The difference Δd between experimental and calculated values for the lattice spacings d corresponding to the $(0,0,10)$ reflection increases with increasing pressure and is correlated with the degree of preferred orientation of the material. This is particularly evident by comparing two diagrams at about 28 GPa from different experiments which differ both in the degree of preferred orientation and in the misfit of the $(0,0,10)$ reflection. One finds differences Δd of 0.002 and 0.005 Å for samples with G_1 parameters of 0.21 and 0.45, respectively. It is likely that above 10 GPa the $Sr_3Fe_2O_7$ samples were increasingly subjected to nonhydrostatic pressure conditions in the nitrogen matrix. After pressure release the preferred orientation remains but the nonuniform stress conditions disappear. Indeed, good agreement between experimental and calculated d values of the $(0,0,l)$ reflections is obtained from the refinement of the diagrams before pressurizing and after pressure release ($\Delta d < 0.0005$ Å in both cases, $G_1 = 0.06$ before pressurizing, $G_1 = 0.43$ after pressure release). These effects mainly influence the accuracy of the c parameters at high pressures, but are not relevant for the main conclusions from this work.

Figure 4 shows the pressure dependence of the unit cell volume V and the tetragonal lattice parameter a. The volume is reduced by about 20% at 45 GPa. The pressure dependence of V can be described by a Birch-Murnaghan equation of state
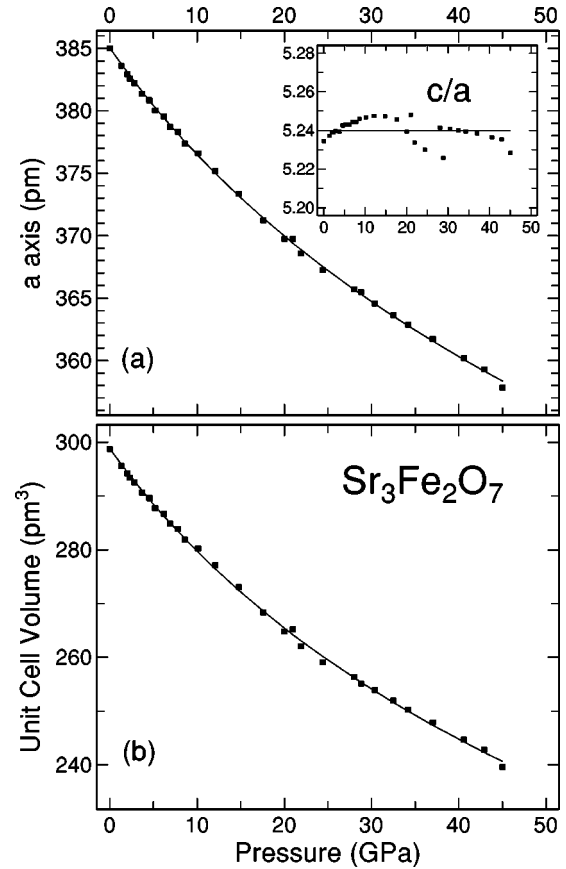
FIG. 4. (a) Lattice parameter a and (b) volume per unit cell V of $Sr_3Fe_2O_7$ as a function of pressure. Solid lines correspond to fitted Birch-Murnaghan relations [see Eq. (2)]. The inset shows the c/a parameter versus pressure.

$$V/V_0 = [1 + (B'/B_0)P]^{-1/B'}, \qquad (2)$$

where V_0, B_0, and B' are volume, bulk modulus, and its pressure derivative at $P = 0$ GPa, respectively. Corresponding equations were used for fitting the pressure dependence of the lattice constants a and c. The fit results listed in Table I and the absence of a significant pressure dependence of the ratio c/a (see inset of Fig. 4) suggest that the compression of $Sr_3Fe_2O_7$ is almost isotropic. Furthermore, the curvature in the compression behavior is rather normal, as is indicated by the fact that the value of B' is close to a value of 4 which is typically observed for low-compressibility solids with (nearly) isotropic elastic properties.

For a discussion of the electronic structure of $Sr_3Fe_2O_7$ under pressure it is desirable to refer to accurate Fe-O bond distances and Fe-O-Fe angles. In this respect, the information which can be derived from the present high-pressure x-ray data is somewhat limited. Due to the small scattering power of oxygen atoms and the small but noticeable nonhydrostatic pressure components it was not possible to extract Fe-O2 and Fe-O3 distances of sufficient accuracy for further discussions. The only Fe-O distances which can be obtained reliably are the Fe-O1 distances. Corner sharing of O1 atoms between adjacent FeO_6 octahedra, leads to the formation of Fe-O1 planes in the crystal structure of $Sr_3Fe_2O_7$. The Fe atoms may be displaced from the center positions of the FeO_6 octahedra, which results in Fe-O1-Fe angles Φ smaller

TABLE I. Parameters obtained from a fit of a Birch-Murnaghan-type equation [see Eq. (2)] to unit cell volume V and lattice parameters a and c of $Sr_3Fe_2O_7$. V_0, a_0, c_0, B_0, B' are the zero-pressure values of volume and lattice constants, the bulk modulus, and its pressure derivative, repectively. The corresponding parameters describing the compression of the axes are denoted as β and β'.

	Parameter	Value
Volume	V_0	$298.76(2) \times 10^6$ pm^3
	B_0	134(6) GPa
	B'	3.8(4)
a axis	a_0	385.02(1) pm
	β_0	387(10) GPa
	β'	12.5(1.1)
c axis	c_0	2015.4(1) pm
	β_0	436(30) GPa
	β'	9.0(2.0)

FIG. 5. Optical reflectance spectra of $Sr_3Fe_2O_7$ at different pressures. The absolute reflectance R_d refers to that measured at the sample-diamond interface (see text for details). The inset shows the reflectance of $Sr_3Fe_2O_7$ measured at 0.6 eV as a function of pressure.

than 180°. The deviation of Φ from 180° at ambient pressure is small ($\Phi = 177°$).[15] Accordingly, half of the lattice parameter a essentially corresponds to the Fe-O1 distance. From the analysis of our x-ray data no systematic trends in Φ with pressure can be established. The mean value of Φ from all diagrams is $173 \pm 3°$. It can thus be assumed that the pressure dependence of $a/2$ (see Fig. 4) basically reflects the pressure dependence of the Fe-O1 distance. As there are no discontinuities in the pressure dependence of a it is concluded that the collapse of the charge disproportionation is not accompanied by major changes in the average Fe-O1 bond lengths. Also above 20 GPa the pressure dependence of the Fe-O1 distances appears to be regular.

C. Optical reflectivity and electrical resistance

Figure 5 shows representative optical reflectance spectra of $Sr_3Fe_2O_7$ between 0.6 and 4 eV for various pressures up to 36 GPa. As noted above, the spectra correspond to the absolute reflectance R_d at the sample-diamond interface. At zero pressure the overall reflectance is low, because the refractive index of the sample is close to that of diamond. Two regions of enhanced reflectivity are observed: one in the near-infrared (NIR) region, the other centered at about 3 eV. The most remarkable result is a major increase of the NIR reflectivity with increasing pressure. This is emphasized in the inset to Fig. 5 where the reflectivity R_d at 0.6 eV is depicted as a function of pressure. The increase in NIR reflectivity is moderate up to 20 GPa and appears to become more pronounced above 20 GPa.

We have simulated the reflectance spectra [see Fig. 6(a)] by using a superposition of Drude-Lorentz oscillators for the complex dielectric function, which is then substituted into the Fresnel equation for the normal incidence reflectivity.[26] An assumption entering into the modeling is that the dielectric properties of $Sr_3Fe_2O_7$ under pressure are nearly isotropic. We allowed for a total oscillator strength below 10 eV, which is similar to that derived from the optical response of other semiconducting TM oxides. This means the effective number of electrons contributing to the imaginary part of the
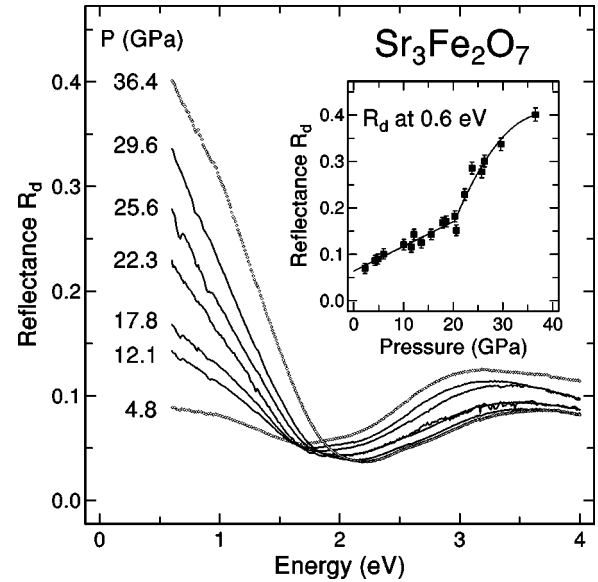
dielectric function has been fixed, such that the integrated optical conductivity between 0 and 10 eV corresponds to an effective electron number of 0.08/Å^3 (for details see Appendix of Ref. 26). In this way we have obtained the frequency dependence of the real part of the optical conductivity shown in Fig. 6(b) for two different pressures. The figure demonstrates that the NIR optical response gains strength under pressure at the expense of transitions at energies above 2 eV. In addition, at 36.4 GPa the real part of the dielectric function changes from negative to positive values at an energy of 1.4 eV. This energy value is tentatively attributed to the screened plasma frequency at this pressure.

The reflectance spectra suggest that the lowest-energy optical excitation gap, indicated by the NIR edge of the optical conductivity at 4.8 GPa [see Fig. 6(b)], becomes smaller at higher pressures. The relatively low NIR reflectance values suggest that a finite excitation gap and an insulating ground state may still persist up to about 20 GPa. The more pronounced increase in NIR reflectivity above 20 GPa is in favor of an insulator-metal transition at higher pressures. In this case the concomitant blueshift of the high-energy cutoff of the NIR reflectance edge (see Fig. 5) is partly attributed to an increase in the screened plasma frequency of the mobile charge carriers.

The temperature-dependent resistance studies provide more direct experimental evidence for the onset of an IM transition with pressure increase. Figure 7 shows resistance versus temperature curves for selected pressures up to 25.8 GPa. The onset of a metallic state is deduced from the change in sign of dR/dT from negative to positive. All the $R(P,T)$ curves beyond ≈ 20 GPa reveal an increase in R with temperature. In the low-temperature region, however, a minimum in R is observed which moves to lower temperatures as pressure is increased. A possible explanation for the low-temperature minimum in R at pressures above 20 GPa is the presence of disorder, which in the limit of weak band
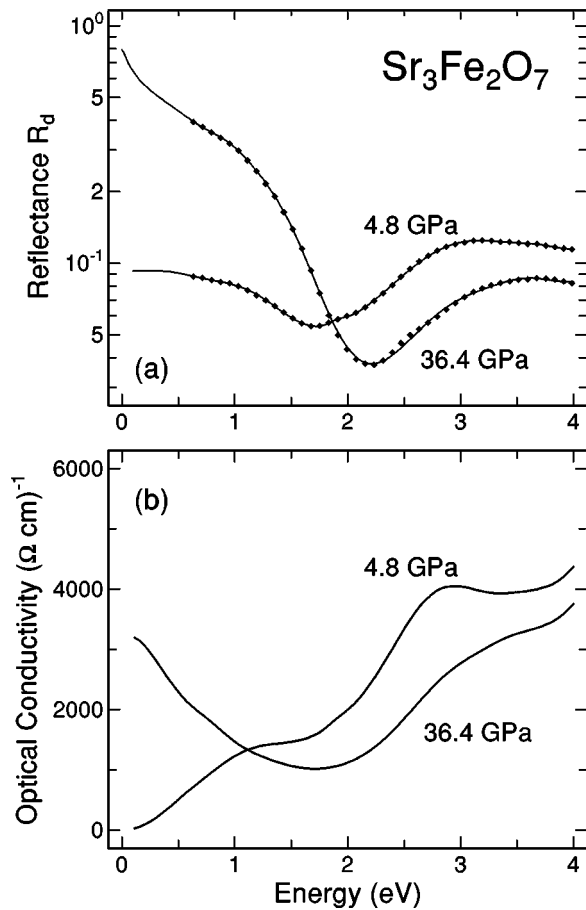
FIG. 6. (a) Reflectance R_d and (b) real part of the optical conductivity of $Sr_3Fe_2O_7$ at 4.8 and 36.4 GPa. Symbols in (a) represent a subset of the experimental data points, solid lines are obtained from fits of an oscillator model (see text) to the experimental spectra.

overlap leads to localization for states near the Fermi level.[31] One may expect these effects to be suppressed at higher pressures due to an increase of the bandwidths and overlap. In fact, the reflectivity spectra (see Fig. 5) clearly evidence a further overall delocalization at pressures above 26 GPa, which is the upper limit of the present transport measurements.

IV. DISCUSSION

The present Mössbauer, optical reflectivity, and electrical resistance measurements evidence a pressure-induced collapse of the charge disproportionation state of $Sr_3Fe_2O_7$ between 12 and 21 GPa and an IM transition near 20 GPa. One would expect that a charge disproportionation will be accompanied by structural modulations like variations in the Fe-O bond lengths. Such a structural manifestation of a charge disproportionation is, e.g., found for $BaBiO_3$.[32,33] Neutron diffraction studies of $Sr_3Fe_2O_7$ did not yield evidence for structural distortions.[15] Also our high-pressure x-ray studies on $Sr_3Fe_2O_7$ do not show any structural anomalies in the pressure range where the charge disproportionation of Fe^{IV} disappears. The space group ($I4/mmm$) remains unchanged and the pressure behavior of the lattice constants appears regular up to 45 GPa. It is concluded that the electronic
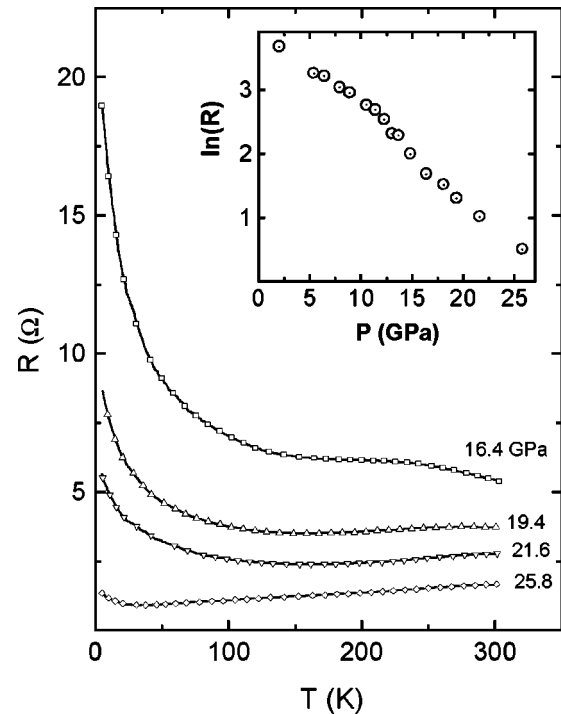
FIG. 7. Resistance R as a function of temperature at selected pressures for $Sr_3Fe_2O_7$. Incipient metallic behavior is evident at $P \geq 20$ GPa. The inset shows the resistance as a function of pressure at 300 K.

structure changes are not accompanied by major changes in the *average* crystal structure. Structural modulations on a microscopic scale like a variation of Fe-O distances at sites with different charges, however, cannot be ruled out. Recent transmission electron microscopy studies revealed a superstructure for the charge-disproportionation phase of $Sr_{0.7}La_{0.3}FeO_3$, a mixed-valence material with formally 70% Fe^{IV} and 30% Fe^{III}.[34]

High-pressure Mössbauer and x-ray diffraction studies on $CaFeO_3$ at room temperature have been interpreted in terms of a first-order high-spin to low-spin transition near 30 GPa which is accompanied by a structural transition from a tetragonal to an orthorhombic phase.[20] The absence of discontinuities in the lattice parameters as well as the absence of significant changes in the character of the Mössbauer spectra in the range 20–45 GPa suggests that there is no major change in the spin configuration of $Sr_3Fe_2O_7$ for pressures up to 45 GPa.

In interpreting the pressure-induced changes in the electronic properties of $Sr_3Fe_2O_7$ we first discuss the ambient-pressure properties of the $Sr_{n+1}Fe_nO_{3n+1}$ series of compounds within the model introduced by Goodenough for rationalizing the electronic behavior of TM compounds.[12] The iron-oxygen network in these materials is built up from corner-sharing regular or nearly regular FeO_6 octahedra. Obviously, there is no evidence for a static Jahn-Teller effect expected for a localized $[t_2(\pi^*)]^3[e(\sigma^*)]^1$ configuration of Fe^{IV}. It is reasonable to assume that the strongly covalent $\sigma^*[e-O(2s,2p_\sigma)-e]$ interactions lead to collective behavior of the σ^* electrons in the semiconducting (Sr_2FeO_4, $Sr_3Fe_2O_7$) as well as in the metallic ($SrFeO_3$) materials.[17] The π^* electrons are considered as localized.
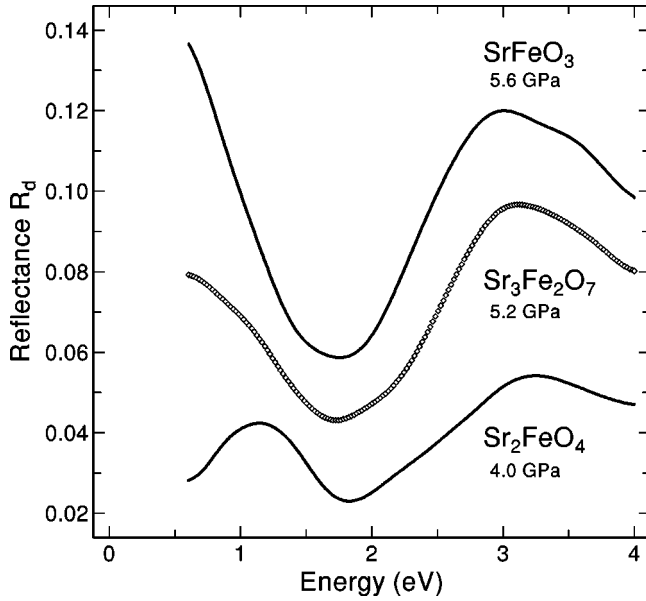
FIG. 8. Comparison of the reflectance spectra of Sr_2FeO_4, $Sr_3Fe_2O_7$, and $SrFeO_3$ measured at low pressures.

The complex electronic behavior of Fe^{IV} oxides is attributed to an electronic ground state at the insulator-metal borderline where the effective electron correlation energy U is of similar size as the width w_σ of the σ^* conduction band.[17] The latter is largest for the cubic perovskite $SrFeO_3$ where metalliclike conductivity is observed. Due to the reduced dimensionality of the Fe-O network w_σ is smaller for Sr_2FeO_4 and $Sr_3Fe_2O_7$. In these two compounds electron-electron correlation and electron-lattice interactions lead to the opening of a gap at the Fermi surface and to the formation of insulating ground states. In $Sr_3Fe_2O_7$ a charge-disproportionation state, which presumably has to be described in terms of charge- and spin-density waves, is stabilized. An intense phonon in the Raman spectra of Sr_2FeO_4 at 380 cm^{-1} (20 K) which cannot be assigned within the ideal K_2NiF_4-type crystal structure[16] and the complex Mössbauer spectra in the magnetically ordered phase[14,15] suggest that the stabilization of an insulating ground state in Sr_2FeO_4 involves a displacement of the Fe atoms from the center positions of the FeO_6 octahedra and the formation of a spin-density wave. A charge disproportionation of Fe^{IV} is not observed for Sr_2FeO_4. The increasing itinerancy of the σ^* electrons in the series Sr_2FeO_4-$Sr_3Fe_2O_7$-$SrFeO_3$ is also seen in the behavior of the NIR reflectance in the low-pressure region (≈ 5 GPa, see Fig. 8). A well-defined NIR band in the reflectance spectra of Sr_2FeO_4 (Ref. 16) corresponds to an optical excitation gap of 1.15 eV. The values of the NIR reflectance of $Sr_3Fe_2O_7$ are enhanced in comparison to Sr_2FeO_4 but smaller than those of $SrFeO_3$.

The absence of discontinuities in the structural parameters of $Sr_3Fe_2O_7$ indicates that the main effect of pressure is a shortening of the average Fe-O distances and therefore a strengthening of the Fe-O-Fe interactions. The concomitant increase in w_σ leads to the closure of the charge-density wave gap and therefore to the collapse of the charge-disproportionation phase as concluded from the Mössbauer spectra above 20 GPa. For $Sr_3Fe_2O_7$ the disappearance of the charge-disproportionation state appears to be associated with an IM transition as is evident from our resistance and optical reflectance data above 20 GPa.

In the case of Sr_2FeO_4 the NIR reflectance starts to increase with pressure above 5 GPa.[16] Furthermore, the additional Raman phonon at 380 cm^{-1} disappears between 5 and 6 GPa and the complex Mössbauer pattern collapses at about 9 GPa.[18] These observations are in agreement with the picture of an electronically driven structural instability and a spin-density wave in Sr_2FeO_4 which both disappear if w_σ is increased. Again, further increase in w_σ due to increasing pressure leads to an IM transition. This is revealed by a dramatic change in the $R(T)$ behavior of Sr_2FeO_4 for $P > 6$ GPa: the temperature variation of R becomes extremely weak albeit with a negative temperature slope.[18] Further increase in bandwidths due to increasing pressure leads to the change in sign of the slope, dR/dT, from negative to positive for pressures at and above $P_c \approx 18$ GPa. Taking into account that for a K_2NiF_4-type crystal structure a pronounced two-dimensional character of the transport properties as well as a possible polaron formation is expected, the change from a positive to a negative temperature coefficient of the conductivity is considered to mark the upper limit for the metallization pressure.

The electronic behavior of Fe^{IV} oxides qualitatively can be well rationalized in terms of the above ''chemical'' model for the electronic properties of TM compounds. For a more quantitative comparison with spectroscopic data the electronic structure of TM compounds is frequently analyzed within an impurity approach considering the hybridization of the $3d$ states of a single TM ion with the ligand (L) p bands.[35] Depending on the relative magnitude of the charge-transfer energy Δ [energy difference between TM($3d$) and $L(p)$ orbitals], the on-site electron correlation energy U, the transfer integrals t_{pd} between TM($3d$) and $L(p)$ orbitals, and the $L(p)$ bandwidth W_p either discrete, insulating, or metallic ground states may occur.[36] The analysis of photoelectron spectra of $SrFeO_3$ (Ref. 13) suggests that the $Sr_{n+1}Fe_nO_{3n+1}$ series of compounds with iron in the high oxidation state +4 belongs to a class of materials with negative effective charge-transfer energy. Accordingly, the wave functions of the insulating as well as of the metallic states of Fe^{IV} oxides are dominated by d^5L^{-1} rather than by ionic d^4 configurations. The energy gap is thus of p-p type and corresponds to charge fluctuations $d^5L^{-1} + d^5L^{-1} \rightarrow d^5 + d^5L^{-2}$, where L^{-1} and L^{-2} denote one and two holes in the oxygen bands, respectively.

Within the impurity approach, high pressure has two opposing effects. On the one hand, increasing values of the transfer integrals t_{pd} due to shortening of the Fe-O distances lead to a stronger intracluster hybridization and to a stabilization of the insulating states in the high-pressure regime. On the other hand, the metallic states are stabilized by the increased intercluster coupling and the increased oxygen bandwidth W_p. In a certain range of parameters a transition from the localized to the itinerant state may occur.[36] Recent MS studies of Sr_2FeO_4 (Ref. 18) show that no change occurs in both the hyperfine field and isomer shift in the pressure range of the IM transition as established from the resistance measurements. This suggests that the Fe $3d$ density of states is essentially unchanged upon metallization, in agreement with the expectations for closure of a p-p-type gap as the

mechanism responsible for the onset of a metallic state. Also for $Sr_3Fe_2O_7$ the average hyperfine field above 15 GPa is nearly pressure independent which again is consistent with the view that the IM transition in this compound proceeds via p-p gap closure.

Within the impurity model the dispersion of the TM $3d$ states is not taken into account explicitly, which, in view of the strong $Fe(3d)$-$O(2p)$-$Fe(3d)$ interactions, appears to be a severe shortcoming. In particular, the charge disproportionation of Fe^{IV} in $Sr_3Fe_2O_7$ and its pressure-driven disappearance point to a more active role of the $3d$ electrons. Rather, a multiband Hubbard approach[37] considering both the dispersional widths of Fe $3d$ and O $2p$ states may be appropriate and is likely to support the chemical considerations. Fe^{IV} oxides like Sr_2FeO_4 and $Sr_3Fe_2O_7$, similar to the Ni^{III} oxides $LnNiO_3$, are examples for TM compounds with an electronic ground state in the covalent-insulator regime.[38] High pressure then induces a covalency-driven insulator-metal transition.

V. CONCLUSIONS

Fe^{IV} oxides are a class of materials where the interplay of strongly covalent $Fe(3d)$-$O(2p)$-$Fe(3d)$ interactions, electron correlation, and electron-lattice interactions leads to unusual electronic states. In the present work we have studied the pressure dependence of the electronic properties and crystal structure of $Sr_3Fe_2O_7$, a compound revealing a charge disproportionation of iron(IV) at ambient pressure. Mössbauer spectroscopy and angle-dispersive synchrotron powder x-ray diffraction studies evidence that the charge disproportionation collapses between 12 and 21 GPa without any structural anomalies. Furthermore, optical reflectivity and electrical resistance experiments show a reduction of the lowest-energy excitation gap under pressure, finally leading to a pressure-driven IM transition at about 20 GPa. Within the model for the electronic properties of TM compounds described by Goodenough in Ref. 12 the σ^* electrons arising from the $[t_2(\pi^*)]^3[e(\sigma^*)]^1$ configuration of Fe^{IV} can be considered as collective electrons. The charge disproportionation gives rise to an energy gain of the system by splitting the quarter-filled σ^* conduction band which opens a charge-density wave gap. In the case of $Sr_3Fe_2O_7$ application of high pressure leads to a strengthening of the covalent $Fe(3d)$-$O(2p)$-$Fe(3d)$ interactions with a concomitant increase in the bandwidth w_σ which results in a collapse of the charge disproportionation and an IM transition. This behavior differs from $CaFeO_3$ where changes in the Mössbauer spectra and crystal structure at room temperature were considered as evidence for a pressure-induced high-spin to low-spin transition.[20] The strongly covalent nature of the insulating as well as of the metallic states in Fe^{IV} oxides is evident from the lack of anomalies in Mössbauer IS and B_{hf} values on passing the IM transition in $Sr_3Fe_2O_7$ and Sr_2FeO_4. Within the impurity model for the electronic structure of TM compounds the IM transition corresponds to a pressure-driven closure of a p-p-type excitation gap.

*Present address: Max-Planck-Institut für Chemische Physik fester Stoffe, Bayreuther Str. 40, D-01187 Dresden, Germany.

[1] D. I. Khomskii and G. A. Sawatzky, Solid State Commun. **102**, 87 (1997).

[2] R. M. Kusters, D. J. Singleton, D. A. Keen, R. McGreevy, and W. Hayes, Physica B **155**, 362 (1989).

[3] R. von Helmolt, J. Wecker, B. Holzapfel, L. Schultz, and K. Samwer, Phys. Rev. Lett. **71**, 2331 (1993).

[4] K. Chahara, T. Ohno, M. Kasai, and Y. Kozono, Appl. Phys. Lett. **63**, 1990 (1993).

[5] R. Mahendiran, A. K. Raychaudhuri, A. Chainani, D. D. Sarma, and S. B. Roy, Appl. Phys. Lett. **66**, 233 (1995).

[6] E. O. Wollan and W. C. Koehler, Phys. Rev. **100**, 545 (1955).

[7] J. B. Goodenough, Phys. Rev. **100**, 564 (1955).

[8] M. Takano and Y. Takeda, Bull. Inst. Chem. Res., Kyoto Univ. **61**, 406 (1983).

[9] P. K. Gallagher, J. B. MacChesney, and D. N. E. Buchanan, J. Chem. Phys. **41**, 2429 (1964).

[10] J. B. MacChesney, R. C. Sherwood, and J. F. Potter, J. Chem. Phys. **43**, 1907 (1965).

[11] T. Takeda, Y. Yamaguchi, and H. Watanabe, J. Phys. Soc. Jpn. **33**, 967 (1972).

[12] J. B. Goodenough, Prog. Solid State Chem. **5**, 145 (1971).

[13] A. E. Bocquet, A. Fujimori, T. Mizokawa, T. Saitoh, H. Namatame, S. Suga, N. Kimizuka, Y. Takeda, and M. Takano, Phys. Rev. B **45**, 1561 (1992).

[14] P. Adler, J. Solid State Chem. **108**, 275 (1994).

[15] S. E. Dann, M. T. Weller, D. B. Currie, M. F. Thomas, and A. D. Al-Rawwas, J. Mater. Chem. **3**, 1231 (1993).

[16] P. Adler, A. F. Goncharov, K. Syassen, and E. Schönherr, Phys. Rev. B **50**, 11 396 (1994).

[17] P. Adler, J. Solid State Chem. **130**, 129 (1997).

[18] G. Kh. Rozenberg, A. P. Milner, M. P. Pasternak, G. R. Hearne, and R. D. Taylor, Phys. Rev. B **58**, 10 283 (1998).

[19] G. Kh. Rozenberg, M. P. Pasternak, A. P. Milner, M. Amanowicz, G. R. Hearne, K. E. Brister, and P. Adler, Rev. High Pressure Sci. Technol. **7**, 653 (1998).

[20] M. Takano, S. Nasu, T. Abe, K. Yamamoto, S. Endo, Y. Takeda, and J. B. Goodenough, Phys. Rev. Lett. **67**, 3267 (1991).

[21] M. Takano, N. Nakanishi, Y. Takeda, S. Naka, and T. Takada, Mater. Res. Bull. **12**, 923 (1977).

[22] S. E. Dann, M. T. Weller, and D. B. Currie, J. Solid State Chem. **97**, 179 (1992).

[23] G. R. Hearne, M. P. Pasternak, and R. D. Taylor, Rev. Sci. Instrum. **65**, 3787 (1994).

[24] A. Hammersley, computer program Fit2D, ESRF, Grenoble, 1997.

[25] J. Rodriguez-Carvajal, ''FullProf: A Program for Rietveld Refinement and Pattern Matching Analysis,'' Abstracts of the Satellite Meeting on Powder Diffraction of the XV Congress of the IUCr, p. 127, Toulouse, 1990.

[26] A. R. Goñi and K. Syassen, in *Semiconductors and Semimetals*

Vol. 54, High Pressure in Semiconductor Physics I, edited by T. Suski and W. Paul (Academic, New York, 1998), p. 248.

[27] G. Kh. Rozenberg, G. R. Hearne, M. P. Pasternak, P. Metcalf, and J. M. Honig, Phys. Rev. B **53**, 6482 (1996).

[28] H. K. Mao, J. Xu, and P. M. Bell, J. Geophys. Res. **91**, 4673 (1986).

[29] P. K. Gallagher, J. B. MacChesney, and D. N. E. Buchanan, J. Chem. Phys. **45**, 2466 (1966).

[30] R. A. Young, in *The Rietveld Method*, edited by P. A. Young (Oxford University Press, Oxford, 1993).

[31] G. Kh. Rozenberg, G. Yu. Machavariani, M. P. Pasternak, A. P. Milner, G. R. Hearne, R. D. Taylor, and P. Adler, Phys. Status Solidi B **211**, 351 (1999).

[32] D. E. Cox and A. W. Sleight, Solid State Commun. **19**, 969 (1976).

[33] D. E. Cox and A. W. Sleight, Acta Crystallogr., Sect. B: Struct. Crystallogr. Cryst. Chem. **35**, 1 (1979).

[34] J. Q. Li, Y. Matsui, S. K. Park, and Y. Tokura, Phys. Rev. Lett. **79**, 297 (1997).

[35] J. Zaanen, G. A. Sawatzky, and J. W. Allen, Phys. Rev. Lett. **55**, 418 (1985).

[36] T. Mizokawa, A. Fujimori, H. Namatame, K. Akeyama, and N. Kosugi, Phys. Rev. B **49**, 7193 (1994).

[37] S. Nimkar, D. D. Sarma, H. R. Krishnamurthy, and S. Ramasesha, Phys. Rev. B **48**, 7355 (1993).

[38] S. R. Barman, A. Chainani, and D. D. Sarma, Phys. Rev. B **49**, 8475 (1994).